High-temperature partitioning of ^{181}Hf-probe impurities between Li and group-V sites in $LiNbO_3$ and $LiTaO_3$

Gary L. Catchen, James M. Adams, and Todd M. Rearick
Department of Nuclear Engineering and Materials Research Laboratory, The Pennsylvania State University, University Park, Pennsylvania 16802
(Received 23 January 1992)

Perturbed-angular-correlation (PAC) spectroscopy was used to measure nuclear-electric-quadrupole interactions at high temperatures in ceramic ternary metal oxides, $LiNbO_3$ and $LiTaO_3$. In these ferroelectric ceramics, the $^{18}Hf \rightarrow {}^{181}Ta$ PAC probe was carried by approximately 0.03 at. % Hf as an impurity dopant, and the PAC measurements were made over a temperature range from approximately 1300 to 1700 K, which included the ferroelectric-to-paraelectric transition for $LiNbO_3$. As we recently reported, at temperatures below ≈ 1100 K, the probe substitutes primarily into the Li sites in both compounds. At higher temperatures, we find that the $^{181}Hf \rightarrow {}^{181}Ta$ probe partitions between the Li and group-V sites. At these higher temperatures, the Li-site electric-field gradients (efg's) are characterized by high frequencies that are similar to those observed at lower temperatures. The group-V site efg's are characterized by frequencies that are approximately one tenth the magnitude of those corresponding to the Li sites. The occupancy of the Li site decreases and that of the group-V sites increases monotonically with increasing temperature. This partitioning is an equilibrium, reversible process that can be described by a simple thermodynamic model of second-order displacement. The temperature dependence of the associated equilibrium constant indicates enthalpies of several eV for the process.

I. INTRODUCTION

In a recent paper,[1] we reported an investigation of nuclear-electric-quadrupole interactions at the Li sites in the ferroelectric, isostructural ceramics $LiNbO_3$ and $LiTaO_3$, which we measured using perturbed-angular-correlation (PAC) spectroscopy via the $^{181}Hf \rightarrow {}^{181}Ta$ probe. The objective of this study was to clarify whether a displacive or an order-disorder mechanism is operative in the ferroelectric-to-paraelectric phase transitions. We found that at temperatures well below the transition temperature T_c, for both $LiNbO_3$ and $LiTaO_3$, the measured spectral lines show extensive broadening and the derived electric-field gradients (efg's) show anomalously large asymmetries. At temperatures above T_c, for $LiTaO_3$, the line broadening decreases and the efg asymmetry is reasonably close to zero. We were able to use Birnie's[2-4] order-disorder model to explain qualitatively the measured temperature dependences of the spectral line broadening and the efg asymmetry. This result supports similar conclusions that were obtained earlier from inelastic Raman spectroscopy performed on $LiNbO_3$ (Ref. 5) and $LiTaO_3$.[6]

In the initial study,[1] we made PAC measurements over a temperature range from 295 to ≈ 1100 K, which included T_c for $LiTaO_3$. Because T_c for $LiNbO_3$ exceeded the accessible temperature range of the apparatus available then, this initial study focused primarily on the features of the $LiTaO_3$ transition. Since then, we developed the capability to make measurements at temperatures up to approximately 1750 K, and we decided to extend the range of measurements on $LiNbO_3$ and $LiTaO_3$ to significantly higher temperatures. We would expect high-temperature measurements on $LiTaO_3$ yield no direct information about the phase transition *per se*. However, the corresponding efg temperature dependence would be useful to know, because, at temperatures below T_c, the efg component V_{zz} increases as temperature approaches T_c even though the corresponding spontaneous polarization P_S decreases.[1] This V_{zz} temperature dependence changes in the opposite direction from those observed on ABO_3 ferroelectric perovskites such as $PbTiO_5$ (Ref. 7) and $BaTiO_3$.[8] For this reason we sought the efg temperature dependence at the Li site in $LiTaO_3$ at temperatures well above T_c. Similarly, we needed to verify whether the temperature dependences both below and above T_c of the spectral line broadening, the efg component V_{zz}, and the asymmetry η are qualitatively similar for isostructural $LiNbO_3$. However, because the melting point of $LiNbO_3$ is only about 50 K above T_c, which is ≈ 1480 K, the available information is inherently limited.

With these considerations in mind we embarked on a series of high-temperature PAC measurements on $LiNbO_3$ and $LiTaO_3$. At temperatures below 1100 K, Hf^{4+} ions at concentrations of $\approx 0.01-0.03$ at. % (of the metal-ion concentrations), which carry the $^{181}Hf \rightarrow {}^{181}Ta$ probe activity, substitute primarily into the Li sites in $LiNbO_3$ and $LiTaO_3$.[1] At higher temperatures, however, sufficient thermal energy is available so that the Hf^{4+} ions can transport between the Li sites and the group-V sites. Thus the experimental information that we intended to seek, namely, the Li-site efg's at high temperatures, is partially obscured by the partitioning of the impurity probe between the Li and the group-V sites. Instead the major effect that we could observe is the temperature dependence of the site occupancy of the $^{181}Hf \rightarrow {}^{181}Ta$

probe. By using a simple equilibrium-thermodynamic model, we could obtain the enthalpies associated with the site changes of the Hf^{4+} probe ions. This information provides a benchmark for theoretical calculations of defect formation energies such as those performed by Donnerberg *et al.*[9]

II. EXPERIMENTAL DETAILS

Ceramic samples of $LiNbO_3$ and $LiTaO_3$, in which the nominal Hf concentrations were approximately 0.03 at. % of the metal-ion concentrations, were prepared using a modified resin-intermediate method.[1] To check the sample phase purity, x-ray powder diffraction patterns were measured on small amounts of powder taken from the radioactive PAC samples. To perform the high-temperature measurements, a special furnace was designed and constructed. Figure 1 presents a schematic diagram of this furnace. Because the temperature control was simple, temperature drifts of 5–10 K during the measurement periods of 1–3 days were observed. On a particular sample, typically, data were collected during a series of experimental runs performed at successively higher temperatures. Then, some runs were performed at lower temperatures to verify that the partitioning of the probe ions between the Li and the group-V sites is reversible. After each series of runs was completed, inspection of the fused-silica sample tube indicated that a small fraction of the sample had chemically reacted with the fused silica. Although both $LiNbO_3$ and $LiTaO_3$ showed this effect, it was more apparent for the $LiTaO_3$ samples, because more of the $LiTaO_3$ runs were performed at higher temperatures than were the $LiNbO_3$ runs. Because the results of lower-temperature runs performed after the higher-temperature runs were in reasonably good agreement with the results of the earlier, lower-temperature runs, for both compounds, we did not consider this effect to be significant.

Reference 1 describes how the PAC measurements and the associated data reduction were generally performed. A minor difference was that the source-to-detector distance was increased from 7 to 10 cm to accommodate the high-temperature furnace. To analyze the measured perturbation functions $A_{22}G_{22}(t)$, a two-site model for nuclear-electric-quadrupole interactions in a polycrystalline source was used:

$$-A_{22}G_{22}(t)=A_1\left[S_0(\eta_1)+\sum_{k=1}^{3}S_k(\eta_1)\exp(-\tfrac{1}{2}\delta_1\omega_k t)\cos(\omega_k t)\right]+A_2\left[S_0(\eta_2)+\sum_{k=4}^{6}S_k(\eta_2)\exp(-\tfrac{1}{2}\delta_2\omega_k t)\cos(\omega_k t)\right]+A_3\ . \quad (1)$$

Here, corresponding to sites one and two, respectively, A_1 and A_2 are the normalization factors, δ_1 and δ_2 are the Lorentzian line-shape parameters. A_3 takes into account the effects of γ rays that are absorbed by the sample and the effects of the fraction of probe atoms that are not in well-defined chemical environments. The frequencies ω_k and the $S_k(\eta)$ coefficients describe a static interaction in a polycrystalline source.[10] Equation (1) was fitted to each measured perturbation function; and the free parameters for site-one (A_1, δ_1, ω_1, ω_2) those for site-two ($A_2,\delta_2,\omega_4,\omega_5$), and A_3 were derived from the fits. For each site, the ratios ω_2/ω_1 and ω_5/ω_4 were used to determine the respective quadrupole frequencies ω_Q. For each site, the nonvanishing efg components V_{ii} in the principal-axis system where the probe nucleus is at the origin are related to the quadrupole frequency ω_Q and the asymmetry parameter η by $\omega_Q=[eQV_{zz}/4I(2I-1)\hbar]$ and $\eta=(V_{xx}-V_{yy})/V_{zz}$, in which Q is the nuclear quadrupole moment (2.51 b) of the spin $I=\frac{5}{2}$ intermediate nuclear level in the ^{181}Ta probe nucleus. The site-occupancy fractions are given by $f_i=A_i/(A_1+A_2+A_3)$, $i=1$, 2, and 3.

III. RESULTS

Figures 2 and 3 present several perturbation functions for $LiNbO_3$ and $LiTaO_3$, respectively. The perturbation functions for both compounds clearly show the contributions from a high-frequency and a low-frequency static interaction. At low temperatures, the high-frequency interaction dominates; and at higher temperatures, the low-frequency interaction dominates. Although the two-site-model fits are reasonably good representations of the data, we suspect, as we described in detail earlier,[1] that the perturbation functions also contain the effects of probe-defect interactions that this model does not take into account. For $LiNbO_3$, the perturbation functions show no large qualitative differences in the character of the high-frequency component. The 1490-K perturbation function, which was measured above T_c, shows a rise in the amplitude of the low-frequency component with increasing time, whereas, the lower-temperature functions do not show this feature. This change could indicate a qualitative change in the site of the low-frequency interaction at temperatures above T_c. However, the temperature range available to explore this effect is limited, especially, since T_c is not known more accurately than perhaps to several tens of degrees. For $LiTaO_3$ neither the high-frequency nor the low-frequency components in the perturbation functions show any significant changes in character over the temperature range of the measurements. All of the $LiTaO_3$ perturbation functions contain a sizable component that corresponds to a fraction of the probes that were not in the site of either the low-frequency or the high-frequency interaction, i.e., f_3 is approximately 0.4. Conversely, the $LiNbO_3$ perturbation functions contain a much smaller component of this type, i.e., f_3 is less than 0.1. This difference could indicate ei-

ther that the Hf^{4+} probe ions are somewhat less soluble in $LiTaO_3$ than in $LiNbO_3$ or that the Hf^{4+} probe ions in $LiTaO_3$ have a higher affinity for trapping defects than they do in $LiNbO_3$. Also, the f_3 magnitudes vary somewhat from sample to sample.

In addition, for both compounds, neither the high-frequency nor the low-frequency interactions produce line-shape changes that would indicate the onset of a time-varying interaction. The static-interaction model, Eq. (1), provides an accurate representation of the measured perturbation functions, and no additional exponential-decay terms, which would represent time-varying effects, are needed to fit the data. Similarly, the A_3 values tend to fluctuate from experimental run to run but these values do not decrease significantly as temperature increases. This result also suggests the absence of time-varying effects.

Figures 4 and 5 summarize the parameters derived from the fits to the $LiNbO_3$ and $LiTaO_3$ perturbation functions. For both $LiNbO_3$ and $LiTaO_3$, the striking effect is that the site-occupancy fractions f_1 and f_2 show monotonic changes with decreasing and increasing temperature, respectively. These changes show that the probe partitions between the site of the high-frequency interaction and the site of the low-frequency interaction. For $LiTaO_3$, there is a decrease in f_1 and a concomitant increase in f_2 occur over a higher temperature range than in the case of $LiNbO_3$. For the high-frequency interaction in $LiNbO_3$, the temperature dependence below T_c of the efg parameters V_{zz} and η and the line-shape parameter δ agree qualitatively with the corresponding temperature dependences for $LiTaO_3$.[1] The efg component V_{zz} increases with increasing temperature. At temperatures below T_c, the asymmetry parameter η is significantly larger than zero, although its behavior above T_c is uncertain; and the line-shape parameter δ is large. At temperatures above T_c, δ decreases, although δ shows

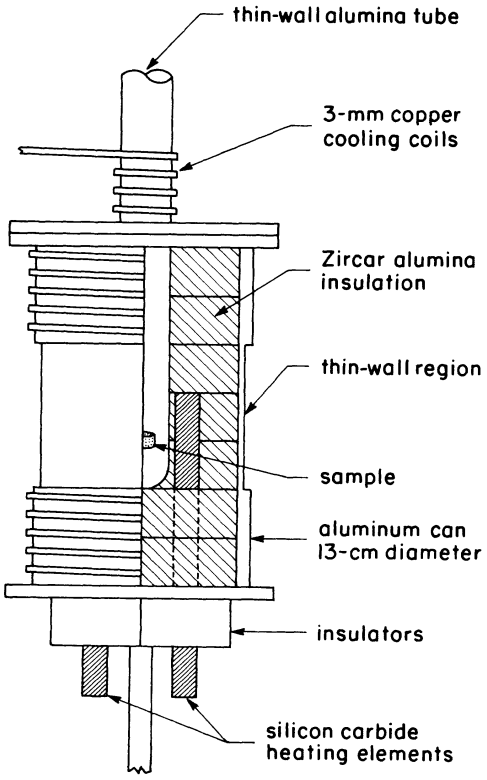

FIG. 1. A schematic diagram of the high-temperature furnace. The furnace consists of four silicon carbide heating elements (custom made by I Squared R Element Co.), several concentric disks of alumina insulation, and an alumina thin wall furnace tube, which are mounted in an aluminum can. The heat is removed primarily by water cooling. The samples may be contained either in fused-silica tubes or attached to a thermocouple with a piece of platinum wire. The γ-ray detectors are usually placed within 1 cm of the outside of the can. The water cooling and appropriately placed heat shields prevent the detectors from becoming excessively hot. The furnace has been operated at temperatures up to 1750 K.

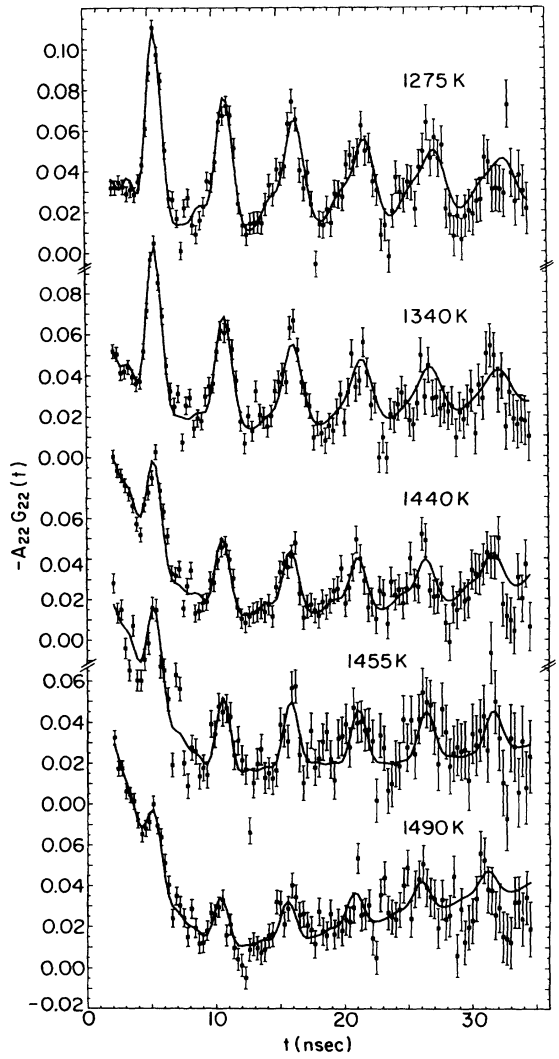

FIG. 2. Perturbation functions for a $LiNbO_3$ samples measured at the indicated temperatures. The solid lines represent least-squares fits of the two-site model equation (1) to the data. The ferroelectric-to-paraelectric transition temperature T_c is approximately 1480 K for $LiNbO_3$.

considerable uncertainties. For the low-frequency interaction in $LiNbO_3$, at temperatures below T_c, V_{zz}, η, and δ show no clear trends. But above T_c, η is significantly displaced from zero. This effect, although somewhat uncertain as we mentioned above, could indicate the effects of the transition to the paraelectric phase. But, an increase in η at temperatures above T_c is not consistent with the symmetry associated with the paraelectric phase, and these large η values could be artifacts. For the high-frequency and low-frequency interactions in $LiTaO_3$, the efg parameters V_{zz} and η and the line-shape parameters δ change very little with temperature, and the presence of large uncertainties obscures any subtle trends that could be present in the data. Additionally, for both $LiNbO_3$ and $LiTaO_3$, the high-frequency interactions measured at the lowest temperature used in this study,

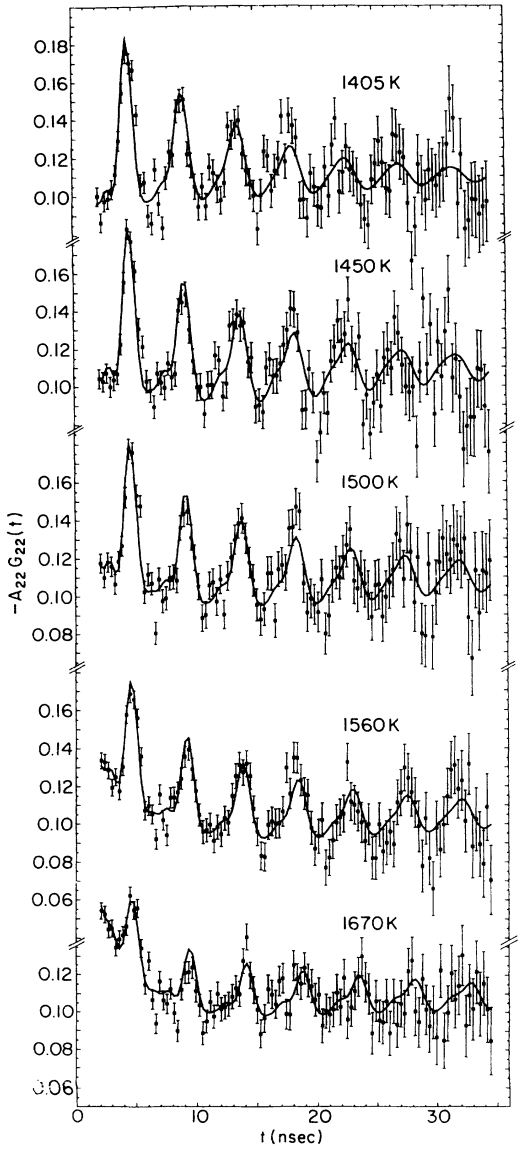

FIG. 3. Perturbation functions for a $LiTaO_3$ sample measured at the indicated temperatures. The solid lines represent least-squares fits of Eq. (1) to the data. For $LiTaO_3$, T_c is approximately 950 K.

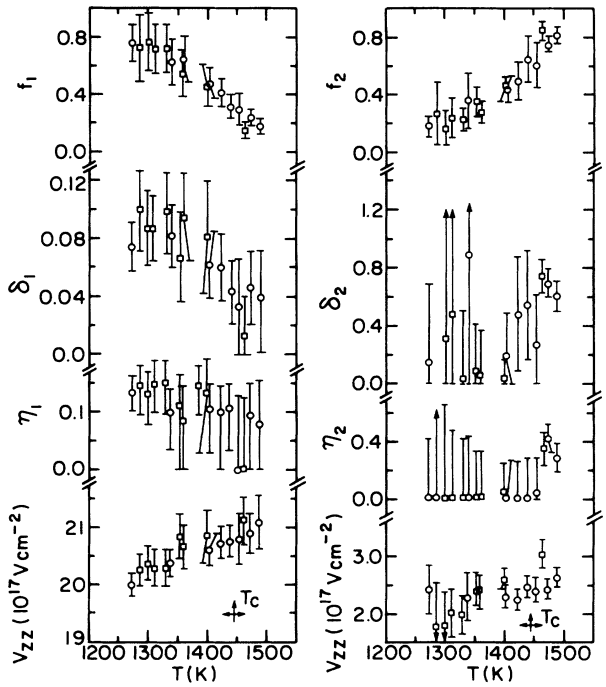

FIG. 4. Electric-field-gradient, line-shape, and site-occupancy-fraction parameters derived from the fits to the $LiNbO_3$ perturbation functions. The two types of data points represent two different ceramic samples that were prepared and measured. The figure on the left side presents the parameters that describe the Li-site interactions, and the figure on the right presents the parameters that represent the Nb-site interactions.

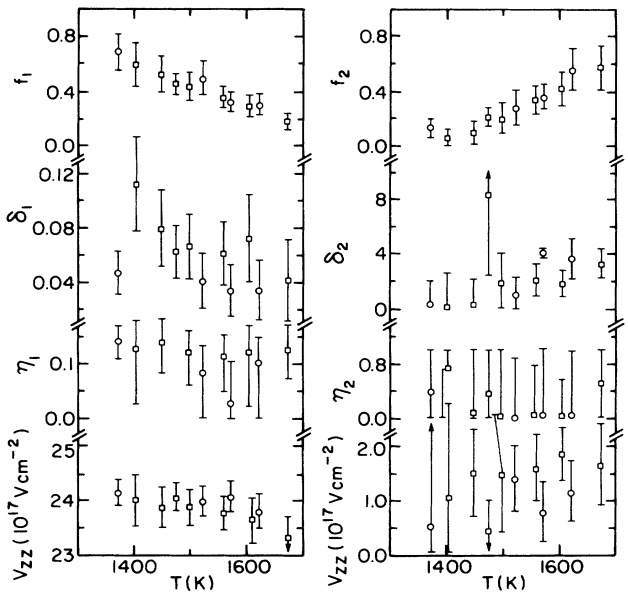

FIG. 5. Electric-field-gradient, line-shape, and site-occupancy-fraction parameters derived from the fits to the $LiTaO_3$ perturbation functions. The two types of data points represent two different ceramic samples that were prepared and measured. The figure on the left side presents the parameters that describe the Li-site interactions, and the figure on the left presents the parameters that represent the Ta-site interactions.

which corresponds to the highest temperature investigated in the previous study,[1] yield parameters that agree well with those reported earlier.[1]

IV. DISCUSSION

A. Site substitution of the probe

During the initial study we determined that at lower temperatures the $^{181}Hf \rightarrow {}^{181}Ta$ probe substitutes primarily into the Li sites in $LiNbO_3$ and $LiTaO_3$ (Ref. 1) and the associated PAC measurements represent nuclear-quadrupole interactions of ^{181}Ta impurity nuclei at those sites. We based this assignment primarily on the results of two different, independent types of experiments: extended x-ray absorption fine-structure spectroscopy[11] was used to determine that Hf^{4+} ions at concentrations of approximately 1 at. % substitute into the Li sites in single crystals of $LiNbO_3$; also, Mössbauer-effect[12] and nuclear-quadrupole-resonance[13] spectroscopies were used to measure the efg temperature dependence at the Ta sites in $LiTaO_3$, and these temperature dependences indicate that the $^{181}Hf \rightarrow {}^{181}Ta$ PAC experiment does not measure the Ta-site efg in $LiTaO_3$ at lower temperatures. For these reasons, the measurements at lower temperatures represent the interactions of Ta^{5+} impurity ions at the Li sites in both $LiNbO_3$ and $LiTaO_3$.

At higher temperatures, as Figs. 4 and 5 show, the population of a second site by the probe increases as temperature increases, and the concomitant population of the first site, which is the Li site, decreases. Although the uncertainties for the second-site parameters are large, the first-site parameters are reasonably well defined. For the second site in $LiTaO_3$, over the temperature range from $\approx 1400-1700$ K, V_{zz} ranges from $(\approx 0.5-2)\times 10^{17}$ V/cm^2 and η and some δ values are for the most part indeterminate. The ^{181}Ta Mössbauer-effect measurements on $LiTaO_3$ yielded $|V_{zz}| \approx 2\times 10^{17}$ V/cm^2 and $\eta \approx 0$ at ≈ 1000 K, above which no data were obtained.[12] Thus the values of V_{zz} and perhaps η for the second site determined from the higher-temperature PAC measurements (>1400 K) are not inconsistent with the values of V_{zz} and η determined from the Mössbauer-effect measurements for the Ta site at a somewhat lower temperature (≈ 1000 K). Moreover, at lower temperatures, group-V antisite defects, e.g., $Nb_{Li}^{\cdots\cdots}$ in Kröger-Vink notation, are relatively common[14] and energetically favored[9] in $LiNbO_3$ and $LiTaO_3$. Thus, forming this antisite defect provides a mechanism to produce group-V-site vacancies $V_{Nb}^{5'}$ and $V_{Ta}^{5'}$. This information strongly suggests that the indicated second-site interactions were measured at the group-V sites in $LiNbO_3$ and $LiTaO_3$.

B. Simple thermodynamic model

As we described above, the $^{181}Hf^{4+}$ probe ions partition between the Li sites and the group-V site. At lower temperatures, below ≈ 1200 K for $LiNbO_3$ and below ≈ 1350 K for $LiTaO_3$, the probe ion occupies primarily the Li site. As temperature increases, the probe ion occupies increasing numbers of group-V sites. This process is reversible; and equilibrium is reached rapidly, during the period in which the sample temperature is adjusted prior to beginning an experimental run.

To describe the process quantitatively, we consider a crystal that has a very small Hf concentration in the presence of large Li and group-V (either Nb or Ta) concentrations. The total number of sites includes equal numbers of Li sites, group-V sites, and interstitial sites. In the diffraction-derived structure, the Li sites and group-V sites are occupied by Li and group-V ions, respectively; and the interstitial sites are vacant.[1] In the real crystal, Hf^{4+}, Li^+, and Nb^{5+} (or Ta^{5+}) ions partition between the Li sites, the group-V sites, and the interstitial sites. The following equations summarize these processes:

$$Li_{Li} = V'_{Li} + Li_I^{\cdot} , \tag{2a}$$

$$Nb_I^{5\cdot} + V_{Nb}^{5'} = Nb_{Nb} , \tag{2b}$$

$$V'_{Li} + Hf'_{Nb} = Hf_{Li}^{3\cdot} + V_{Nb}^{5'} , \tag{2c}$$

in which "Nb" represents the group-V ion Nb^{5+} or Ta^{5+}. The net reaction is given by

$$Nb_I^{5\cdot} + Hf'_{Nb} + Li_{Li} = Nb_{Nb} + Li_I^{\cdot} + Hf_{Li}^{\cdots} . \tag{2d}$$

The corresponding mass-action expression is

$$K = [Li_I^{\cdot}][Nb_{Nb}][Hf_{Li}^{3\cdot}]/[Nb_I^{5\cdot}][Li_{Li}][Hf'_{Nb}] , \tag{3}$$

in which K is the equilibrium constant. Since the Hf concentrations are small compared to the Li and group-V concentrations, we can make the approximation $[Li_{Li}] \approx [Nb_{Nb}]$; and the resulting expression for the equilibrium constant is

$$K \approx [Li_I^{\cdot}][Hf_{Li}^{\cdots}]/[Nb_I^{5\cdot}][Hf'_{Nb}] . \tag{4}$$

Since $[Nb_I^{5\cdot}] \approx [Hf'_{Nb}]$ and $[Li_I^{\cdot}] \approx [Hf_{Li}^{\cdots}]$, Eq. (4) reduces to

$$K^{1/2} \approx [Hf_{Li}^{\cdots}]/[Hf'_{Nb}] . \tag{5}$$

The ratio of the normalization factors in Eq. (1) (A_1/A_2) is equal to ($[Hf_{Li}^{\cdots}]/[Hf'_{Nb}]$) in Eq. (5). For the process that Eq. (2d) indicates, the equilibrium constant is related to the standard-state Gibbs-free-energy change ΔG° by $K^{1/2} = \exp(-\Delta G^\circ/2kT)$, in which k is the Boltzmann constant. The resulting expression is

$$\ln(A_1/A_2) = (\Delta S^\circ/2k) - (\Delta H^\circ/2k)(1/T) , \tag{6}$$

in which ΔS° and ΔH° are the standard-state entropy and enthalpy changes associated with ΔG°. Figures 6 and 7 show fits of Eq. (6) to the experimentally determined ratios A_1/A_2 for $LiNbO_3$ and $LiTaO_3$, respectively. The corresponding enthalpies and entropies are $\Delta H^\circ = 4\pm 1$ eV and $\Delta S^\circ = (3.2\pm 0.1)\times 10^{-3}$ eV/K and $\Delta H^\circ = 5\pm 1$ eV and $\Delta S^\circ = (3.0\pm 0.1)\times 10^{-3}$ eV/K. We estimated the uncertainties by using limiting slopes determined by eye.

Although the ratios A_1/A_2 have considerable uncertainties associated with them, the linear fits of Eq. (6) are reasonably good representations of the data. The derived

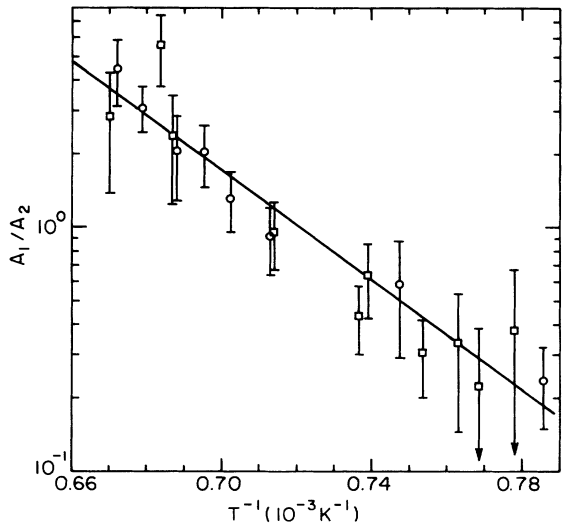

FIG. 6. Logarithmic dependence of the site-occupancy ratio A_1/A_2 on inverse temperature for $LiNbO_3$. The line represents a least-squares fit to the data.

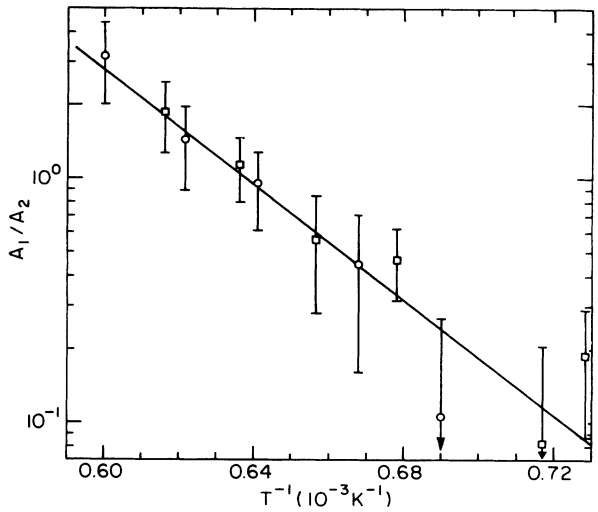

FIG. 7. Logarithmic dependence of the site-occupancy-ratio A_1/A_2 on inverse temperature for $LiTaO_3$. The line represents a least-squares fit to the data.

enthalpy values, which are approximately 3–6 eV, are consistent with the energies for forming group-V Frenkel-pair defects ($V_{Nb}^{5'}+Nb_I^{5\cdot}$) in $LiNbO_3$ that Donnerberg *et al.*[9] calculated. However, this thermodynamic model, which Eqs. (2a)–(2d) describe, is not necessarily unique. Moreover, this model implies that probe-ion transport is a second-order process, i.e., the kinetics are bimolecular. For a Hf^{4+} ion to move from a Li site to a group-V site, a group-V ion must vacate a group-V site nearby. Subsequently a Li^{1+} ion must move into the Li site that the Hf^{4+} ion vacated. As a result, the derived enthalpies ΔH° represent the net energy change associated with this process, which Eq. (2d) represents. These features of the model imply that large concentrations of defects in the crystals, which are well known to occur,[14] do not strongly affect the transport of the Hf^{4+} probe ions between the Li and group-V sites. Defects such as V'_{Li} and $Nb_{Li}^{\cdots}$ and $Ta_{Li}^{\cdots}$ are present in $LiNbO_3$ and $LiTaO_3$. But in the context of the model, the primary process of Hf^{4+} ions moving between Li and group-V sites appears to involve Hf^{4+} ions displacing either group-V ions at group-V sites or Li ions at Li sites as opposed to Hf^{4+} ions moving from either a Li site or a group-V site to either a $V_{Nb}^{5'}$ or a $V_{Ta}^{5'}$ or a V'_{Li}. Additionally the partitioning of the probe between the sites is relatively insensitive to the details of the ferroelectric-to-paraelectric phase transitions. For $LiNbO_3$ T_c is about 500 K higher than T_c is for $LiTaO_3$, yet, the measurable onset of the transport of the Hf^{4+} ions from the Li sites to the Nb sites in $LiNbO_3$ occurs at somewhat lower temperatures than does the corresponding process in $LiTaO_3$.

V. CONCLUSIONS

At high temperatures static nuclear-electric-quadrupole interactions were measured at the Li sites and the group-V sites in $LiNbO_3$ and $LiTaO_3$ using the $^{181}Hf \rightarrow {}^{181}Ta$ PAC probe. As temperature increases the occupancy of the Li sites by the Hf^{4+} probe ions decreases monotonically, and the occupancy of the group-V site increases commensurately. The transport of the probe ion between the Li and the group-V sites is an equilibrium, reversible process that can be described by a simple thermodynamic model. This model indicates that the probe-ion transport is primarily a second-order process. The temperature dependence of the associated equilibrium constant yields reasonable values for the enthalpy and entropy for the process.

ACKNOWLEDGMENTS

We thank Professor William B. White and Dr. Ian D. Williams of the Materials Research Laboratory and Professor Dunbar P. Birnie III of the University of Arizona for sharing their insights into thermodynamic models of defect chemistry. We thank Mr. David M. Spaar and Ms. Maria C. Fonseca for helping us with preparing and characterizing samples. We thank Professor Wayne Huebner of the University of Missouri-Rolla for suggesting the initial design of the high-temperature furnace. We thank Professor James F. Scott of the University of Colorado for calling our attention to several important studies of phase-transition mechanisms in $LiNbO_3$ and $LiTaO_3$. We gratefully acknowledge support from the Office of Naval Research (Grant No. N00014-90-J-4112).

[1]G. L. Catchen and D. M. Spaar, Phys. Rev. B **44**, 12 137 (1991).
[2]D. P. Birnie III, J. Mater. Res. **5**, 1933 (1990).
[3]D. P. Birnie III, J.Am. Ceram. Soc. **74**, 988 (1991).
[4]D. P. Birnie III, J. Appl. Phys. **69**, 2485 (1991).
[5]Y. Okamoto, P. Wang, and J. F. Scott, Phys. Rev. B **32**, 6787 (1985).
[6]M. Zhang and J. F. Scott, Phys. Rev. B **34**, 1880 (1986).
[7]G. L. Catchen, S. J. Wukitch, D. M. Spaar, and M.

Blaszkiewicz, Phys. Rev. B **42**, 1885 (1990).
[8]G. L. Catchen, S. J. Wukitch, E. M. Saylor, W. Huelner, and M. Blaszkiewicz, Ferroelectrics **117**, 175 (1991).
[9]H. Donnerberg, S. M. Tomlinson, C. R. A. Catlow, and O. F. Schirmer, Phys. Rev. B **40**, 11 909 (1989).
[10]For more information about the analysis of nuclear-electric-quadrupole interactions in polycrystalline sources, see, for example, G. L. Catchen, J. Mater. Educ. **12**, 253 (1990); G. L. Catchen, Hyperfine Interactions **52**, 65 (1989).
[11]C. Prieto, C. Zaldo, P. Fessler, H. Dexpert, J. A. Sanz-García, and E. Diéguez, Phys. Rev. B **43**, 2594 (1991).
[12]M. Löhnert, G. Kaindl, G. Wortmann, and D. Salomon, Phys. Rev. Lett. **47**, 194 (1981).
[13]A. P. Zhukov, L. V. Soboleva, L. M. Belyaev, and A. F. Volkov, Ferroelectrics **21**, 601 (1978).
[14]S. C. Abrahams and P. Marsh, Acta Crystallogr. B **42**, 61 (1986).